metals

MDPI

Article

Age-Induced Precipitation and Hardening Behavior of Ni_3Al Intermetallic Alloys Containing Vanadium

Satoshi Semboshi [1,*], Ryosuke Sasaki [2], Yasuyuki Kaneno [2] and Takayuki Takasugi [2]

[1] Institute for Materials Research, Tohoku University; Katahira 2-1-1, Aoba-ku, Sendai, Miyagi 980-8577, Japan
[2] Department of Materials Science, Osaka Prefecture University; Gakuen-cho 1-1, Naka-ku, Sakai, Osaka 599-8531, Japan; idhxk40272@yahoo.co.jp (R.S.); kaneno@mtr.osakafu-u.ac.jp (Y.K.); takasugi@mtr.osakafu-u.ac.jp (T.T.)
* Correspondence: semboshi@imr.tohoku.ac.jp; Tel.: +81-22-215-2220

Received: 25 December 2018; Accepted: 30 January 2019; Published: 1 February 2019



Abstract: $L1_2$-type Ni_3Al alloys containing vanadium are potential candidates for solid-solution and age-hardenable alloy systems, according to the Ni_3Al-Ni_3V pseudo-binary phase diagram. Therefore, herein, variations in the microstructure and mechanical properties of Ni-13 at.% Al-12 at.% V-50 ppm B alloy during isothermal aging were investigated. Alloy specimens were solution-treated at 1323 K for 48 h, quenched in water, and aged at 1073 K to 1173 K. The quenched specimens exhibited a single phase of Ni_3Al ($L1_2$ structure derived from Al (fcc) structure), while in the aged specimens, numerous fine disk-shaped precipitates identified as Ni_3V ($D0_{22}$ structure from orthorhombic structure) were formed on {001} planes of the Ni_3Al matrix. The size of the disk-shaped Ni_3V precipitates increased gradually with increasing aging period. The hardness and strength of the specimens increased initially during aging at 1073 K to 1173 K, reached a maximum, followed by a subsequent decrease. The age-hardening behavior observed for the specimens can be explained in terms of precipitation of the fine disk-shaped Ni_3V precipitates in the Ni_3Al matrix. Furthermore, the peak-aged specimens exhibited an increase in yield strength with increasing testing temperature, similar to other $L1_2$-type intermetallic alloys.

Keywords: Ni_3Al; vanadium; aging; microstructure; precipitation; strength

1. Introduction

Ni_3Al-based alloys offer several advantages such as high melting point, excellent mechanical properties at high temperatures, high thermal conductivity, good oxidization resistance, and low density, which are prerequisites for the vehicle components used in high-temperature applications such as engines and turbine blades. With the development of novel high-temperature materials, Ni_3Al intermetallic compounds with the $L1_2$ structure derived from the A1 (fcc) structure play an important role as the primary phase for single-phase Ni_3Al-based alloys, [1–11] Ni_3Al/Ni_3V for dual two-phase alloys [12–15], and the dispersive strengthening phase for Ni-based superalloys [16–20]. However, Ni_3Al-based alloys suffer from poor ductility at ambient temperature and therefore, fundamental and practical efforts to improve not only the strength at low and high temperatures but also the intrinsic deformability of the Ni_3Al phase have been of significant interest.

In order to provide an excellent combination of mechanical properties of Ni_3Al-based alloys, the Ni_3Al phase should be modified by alloying and microstructural optimization. For example, a drastic increase in the ductility of Ni_3Al obtained by boron doping has been reported [21–24]. Further, there have been numerous investigations on Ni_3Al-based alloys strengthened by solid-solution hardening via the elemental addition of Ti, Cr, Nb, and Ta [25–27]. There have also been studies on alloys strengthened by the dispersion of soft precipitates of a Ni solid solution [28,29], and hard

particles such as ceramics and oxides [30–32]. However, to meet the current requirement of high-performance components, further enhancement of the mechanical, and physical properties of Ni_3Al-based alloys is crucial.

Alloys based on the Ni_3Al-Ni_3V pseudo-binary alloy system should be potential solid-solution and aged-hardenable alloys, because vanadium dissolves well in the $L1_2$ Ni_3Al phase and largely supersaturates at a eutectoid temperature, as shown in Figure 1 [33]. It is also expected that age-induced hardening due to the precipitation of hard Ni_3V with the $D0_{22}$ structure can improve the strength without significant degradation of other properties, such as thermal conductivity and environmental resistance [34,35]. The mechanical properties of Ni_3Al alloys were improved by adding 1–2 at.% of vanadium [26,27]; however, there is no study on the mechanical properties of Ni_3Al alloys containing a large amount of vanadium. Further, there have only been few reported attempts to demonstrate the age-hardening behavior in the Ni_3Al-Ni_3V system. Hence, in this study, we strengthened Ni_3Al alloys through the fine dispersion of age-induced precipitates, as well as through the dissolution of solutes in the matrix, by which the dislocation motion was hindered even at high temperatures. We then examined variations in the microstructure and mechanical properties during isothermal aging for a Ni_3Al alloy containing a large amount of vanadium.

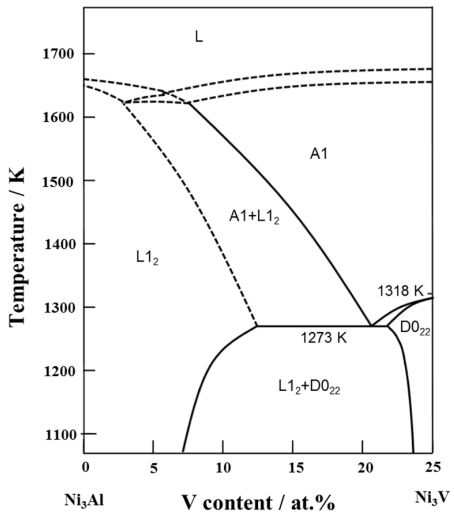


Figure 1. Ni_3Al–Ni_3V pseudo-binary phase diagram adapted from [33], with permission from Elsevier, 2012.

2. Materials and Methods

Based on the phase diagram of the Ni_3Al–Ni_3V pseudo-binary alloy system (Figure 1; [33]), single-phase $L1_2$ Ni_3Al alloys with the nominal composition of Ni-25 at.% Al-50 wt. ppm B and Ni-13 at.% Al-12 at.% V-50 wt. ppm B were prepared. Here, a small amount (50 wt. ppm) of B was doped on both alloys in order to improve the ductility of the parent Ni_3Al phase through the suppression of intergranular fracture [21–24]. Hereafter, these alloys are denoted as Ni_3Al-0V and Ni_3Al-12V alloys, respectively. Alloy button ingots with a diameter of 30 mm or 50 mm were fabricated by arc-melting in argon atmosphere using a non-consumable tungsten electrode on a copper hearth. Pure nickel grains (99.99 wt.% in purity), aluminum tips (99.9 wt.%), vanadium grains (99.9 wt.%), and boron powder (99.9 wt.%) were used as raw materials. The button ingots were melted repeatedly at least four times to ensure complete chemical homogeneity, and were then cut into sample pieces using an electro-discharge machine. After the contaminated layer was removed from the specimen surface by mechanical grinding, the pieces were encapsulated in a quartz tube, in which the pressure was maintained to be less than 2.0×10^{-3} Pa. Subsequently, the encapsulated specimens were heat-treated at 1323 K for 48 h and quenched in water, to obtain single-phase $L1_2$ Ni_3Al with and without vanadium. Some Ni_3Al-12V alloy specimens were encapsulated again under a vacuum of less than 2.0×10^{-3} Pa

in a quartz tube, and then isothermally aged at 1073 K, 1123 K, and 1173 K for various durations from 1 h to 240 h, followed by quenching in water.

The microstructures of the specimens were investigated by conventional field-emission scanning electron microscopy (FESEM) using a JSM-7001F (JOEL Inc., Tokyo, Japan),, and transmission electron microscopy (TEM) using a JEM-2000FX (JOEL Inc., Tokyo, Japan) operated at an accelerating voltage of 200 kV. Specimens for TEM observations were first mechanically abraded to less than 30 μm in thickness using SiC paper, and then polished by low-angle ion milling using a PIPS (Gatan Inc., Tokyo, Japan) with an argon ion beam accelerated at 3.5 kV. Hardness measurements were carried out using a Vickers microhardness tester HM-101 (Mitsutoyo Inc., Tokyo, Japan) under an applied load of 4.9 N for a dwell time of 10 s. The average hardness was obtained from more than 10 indentations. Tensile tests were performed using a universal tensile testing machine TENSIRON UTA-10 KN (A&D Co. Ltd., Tokyo, Japan) at temperatures ranging between room temperature (298 K) and 1073 K with an initial strain rate of 1.67×10^{-4} s^{-1} under a vacuum of less than 2.0×10^{-3} Pa. For the tensile tests, dog-bone-shaped specimens with a cross-section of 2 mm × 1.5 mm and gauge length of 10 mm were used.

3. Results and Discussion

3.1. Microstructure

Figure 2 shows typical FESEM and bright-field (BF) images and a corresponding selected-area electron diffraction (SAED) pattern of the Ni_3Al-12V alloy specimen quenched from 1323 K. The specimens obtained through casting, annealing, and then quenching comprise relatively coarse grains with sizes ranging from 100 μm to 1 mm, as observed in Figure 2a. There are no contrasts from second phases in the matrix phase (Figure 2a,b), although few strain contrasts from dislocations are observed in Figure 2b. The SAED pattern (Figure 2c), which was taken from the matrix phase, indicates that all the fundamental and superlattice reflections can be indexed to the $L1_2$ structure of the Ni_3Al phase (lattice parameter, a = 0.356 nm), as illustrated schematically in Figure 2d. Thus, we confirmed that the Ni_3Al-12V alloy specimen quenched from 1323 K comprised a single phase of $L1_2$ Ni_3Al containing vanadium element. This indicates that the solubility limit of vanadium for the $L1_2$ Ni_3Al phase at 1323 K (Figure 1) should be more than 12 at.%.

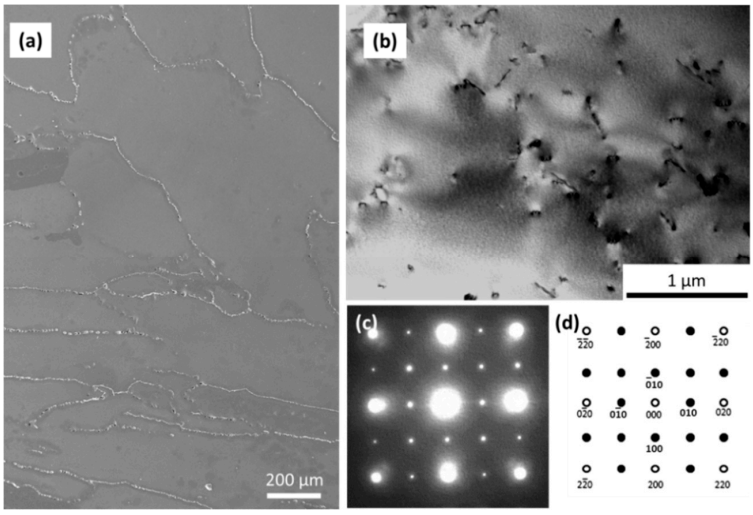


Figure 2. (**a**) Field-emission scanning electron microscopy (FESEM) image and (**b**) bright-field (BF) transmission electron microscope (TEM) image of the Ni_3Al-12V alloy quenched from 1323 K. (**c**) A selected-area electron diffraction (SAED) pattern taken from the matrix. (**d**) Schematic illustration of the SAED pattern, viewed from the [001] zone axis of the $L1_2$ structure. The fundamental and superlattice reflections from the $L1_2$ structure are marked by open and filled circles, respectively.

Figure 3a shows a BF image of the Ni_3Al-12V alloy specimen isothermally aged at 1123 K for 4 h. The incident beam direction is close to the $[001]_m$ zone axis (the subscript "m" denotes the $L1_2$ Ni_3Al matrix phase). We can see dark contrasts, with a length of approximately 1 μm, extended preferentially along the $[100]_m$ and $[010]_m$ directions, as indicated by the arrows in Figure 3a. Figure 3b shows a SAED pattern taken from the extended dark contrasts (dotted circle in Figure 3a). The SAED pattern was identified by a superposition of reflections from the $L1_2$ Ni_3Al matrix shown in Figure 2c, and the Ni_3V with a $D0_{22}$ structure from the orthorhombic structure with lattice parameters a = 0.355 nm and c = 0.719 nm, as marked by the diamond shapes in Figure 3c. Thus, the precipitates introduced by aging at 1123 K were identified as $D0_{22}$ Ni_3V, which was predicted from the phase diagram of Figure 1. The orientation relationship between the Ni_3Al matrix and Ni_3V precipitates was $[001]_m//[001]_p$, $(100)_m//(100)_p$ (the subscript "p" denotes the precipitate phase of Ni_3V with a $D0_{22}$ structure).

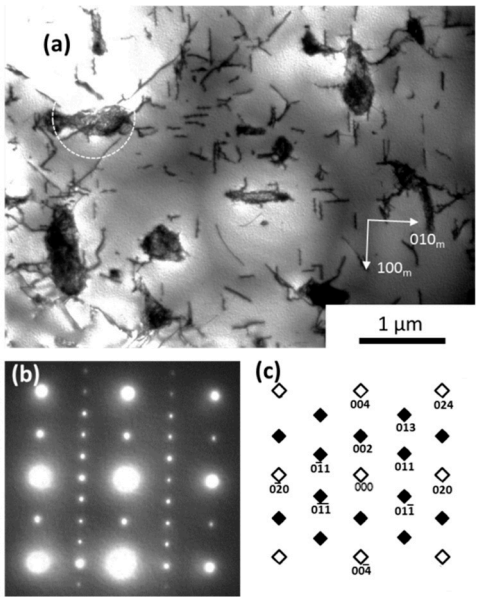


Figure 3. (**a**) Bright-field (BF)-TEM image of the Ni_3Al-12V alloy aged at 1023 K for 4 h, viewed from the [001] zone axis of the matrix with a $L1_2$ structure. (**b**) SAED pattern taken from the area with a dark elliptical contrast as marked by the dotted circle in (**a**). (**c**) Schematic illustration of the SAED pattern viewed from the [100] zone axis for $D0_{22}$ structure [15]. The fundamental and superlattice reflections from the $D0_{22}$ structure are marked by open and filled diamonds, respectively.

Figure 4 shows the BF images of the Ni_3Al-12V alloy specimen isothermally aged at 1123 K for 16 h and 48 h. The incident beam direction is close to the $[001]_m$ zone axis. We can see dark contrasts from Ni_3V precipitates, which extend preferentially along the $[100]_m$ and $[010]_m$ directions, similar to those in Figure 3a. There are two shapes of contrasts of the Ni_3V precipitates; i.e., extended elliptical (indicated by arrows in Figure 4b) and almost circular (dotted circle) ones. This suggests that the $D0_{22}$ Ni_3V precipitates in the $L1_2$ Ni_3Al matrix should be dispersed preferentially along $(001)_m$ with a disk-like shape (Figure 5). The size and aspect ratio of the Ni_3V precipitates appear to increase with aging time. The diameter is approximately 1.5 μm for 16 h of aging and 2 μm for 48 h of aging; both exhibit a similar thickness of 0.5 μm. Here, the misfit strains along the a- and c-axes on the matrix plane with the precipitates are estimated to be approximately 0.3% and 0.8%, respectively, because the lattice parameters of $L1_2$ Ni_3Al and $D0_{22}$ Ni_3V in the two-phase region have been reported as a = 0.356 nm, and a = 0.355 nm, and c = 0.719 nm respectively [36]. Therefore, the disk-like two-dimensional growth of $D0_{22}$ Ni_3V precipitates, which have coherent broad faces on the $(001)_m$ planes containing the a- and b-axes of the matrix, should be caused by the minimization of the interface energy between the $L1_2$ Ni_3Al matrix and the $D0_{22}$ Ni_3V precipitates [37].

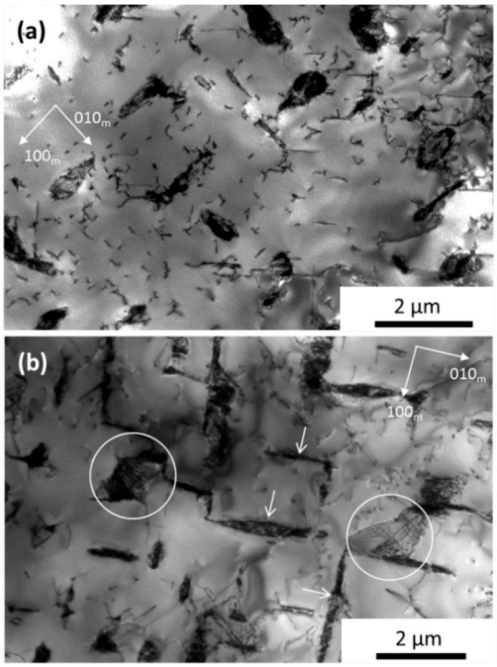


Figure 4. BF-TEM images of the Ni_3Al-12V alloy aged at 1023 K for (**a**) 16 h (peak-hardened condition) and (**b**) 48 h, viewed from the [001] zone axis of the matrix with the $L1_2$ structure.

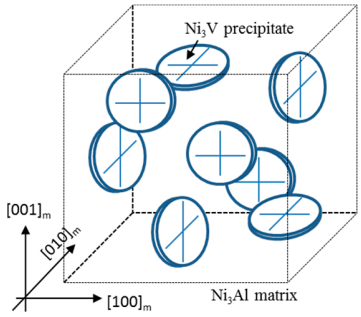


Figure 5. Schematic illustration of $D0_{22}$ Ni_3V precipitates in an $L1_2$ Ni_3Al matrix grain for the aged Ni_3Al-12V alloy specimen. Disk-like shaped Ni_3V precipitates are dispersed on $\{001\}_m$ planes with a crystallographic orientation relationship, $[001]_m//[001]_p$, $(100)_m//(100)_p$ between the matrix and precipitates.

3.2. Mechanical Properties

Figure 6 shows the variation in the Vickers hardness of the Ni_3Al-12V alloy specimens during isothermal aging at 1073 K, 1123 K, and 1173 K. The hardness for all three aging temperatures increases initially, reaches a maximum value, and then decreases for the specimens that underwent prolonged aging. The value of the maximum hardness decreases with increasing aging temperature, while the period to reach the maximum hardness is shortened.

The age-hardening behavior might be common with some conventional age-hardenable Al, Cu, and Fe alloy systems [38–41], and can be, in this case, explained by the precipitation of $D0_{22}$ Ni_3V. In the initial stage of aging, the hardness steadily increased with the nucleation and growth of $D0_{22}$ Ni_3V precipitates in the $L1_2$ Ni_3Al matrix phase. The maximum hardness is associated with the maximum number of $D0_{22}$ Ni_3V precipitates. This implies that the continuous nucleation of $D0_{22}$ Ni_3V precipitates is saturated, due to the depletion of super-saturated solid-solute vanadium atoms in the matrix. The hardness decreases with further aging due to an increase in the distance between the $D0_{22}$ Ni_3V precipitates, which might be because the precipitates undergo Ostwald ripening, like other age-hardenable alloys [38,39,41].

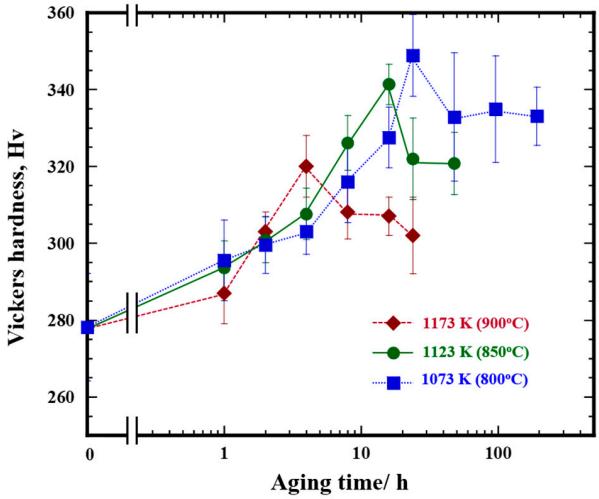


Figure 6. Variation in Vickers hardness with aging time for the Ni_3Al-12V alloy specimens aged at 1073 K, 1123 K, and 1173 K. The measured hardness of the as-quenched specimen is 278 Hv.

Figure 7 shows the typical nominal stress-strain curves at 298 K for the Ni_3Al-12V alloy specimens quenched and peak-aged at 1123 K for 16 h, together with the quenched Ni_3Al-0V alloy specimen for comparison. The quenched Ni_3Al-0V alloy yields with mild plastic elongation, which is consistent with previous reports [2,7,10]. On the other hand, both, the quenched and aged Ni_3Al-12V alloy specimens show a greater yield strength than the quenched Ni_3Al-0V alloy specimen, followed by extensive work hardening accompanied by a larger fracture strain. The enhancement in yield strength for both specimens should be attributed primarily to solid-solution hardening by the vanadium atom dissolved in the $L1_2$ Ni_3Al phase. Mishima et al. reported an increased rate of change in solid-solution hardening per atomic percent, ($d\sigma/dc$), for vanadium [27]. However, the detailed influence of a large amount of vanadium dissolving in the Ni_3Al phase on the mechanical properties is still unclear. We are systematically investigating this and will report it in the future. The yield strength of the peak-aged Ni_3Al-12V alloy specimen seemed to be slightly greater by 15 MPa than that of the quenched Ni_3Al-12V alloy specimen. This must be due to the age-induced precipitates of $D0_{22}$ Ni_3V in the $L1_2$ Ni_3Al matrix phase. Nevertheless, yield strengthening by the age-induced precipitates should not be as significant as strengthening by the solid-solution effect of vanadium atoms.

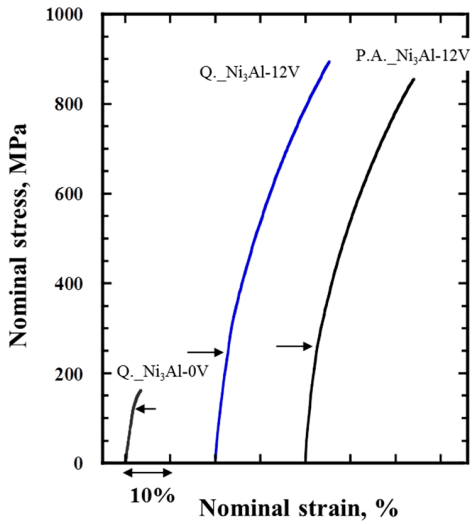


Figure 7. Nominal stress versus nominal strain curves for the quenched (Q.) Ni_3Al-0V and Ni_3Al-12V alloy specimens, and peak-aged (P.A.) Ni_3Al-12V alloy aged at 1123 K for 16 h.

Figure 8 shows the typical nominal stress-strain curves at elevated temperatures from 298 K to 1073 K for the Ni_3Al-12V alloy specimens peak-aged at 1123 K for 16 h. The 0.2% yield strength is shown by arrows in Figure 8. Figure 9 summarizes the yield strength (0.2% proof stress), ultimate tensile strength, and fractural strain for the Ni_3Al-12V alloy specimens quenched and peak-aged at 1123 K for 16 h as a function of the testing temperature. In comparison to the stoichiometric Ni-25 at.% Al binary alloy [10], the yield strengths of the quenched and peak-aged Ni_3Al-12V alloy specimens at 298 K are higher, as described above. Notably, the yield strength of both specimens steadily increases with the testing temperature to 1073 K, indicating an anomalous temperature dependency of yield strength, similar to other $L1_2$ intermetallic compounds [1,2,42], while that of the stoichiometric Ni_3Al binary alloy specimen shows a peak at around 800 K. The peak temperature at which the maximum flow strength is observed has been suggested to be associated with the transition of the slip system with temperature [3,43]. Accordingly, the result observed in Figure 9a indicates that the transition temperature of the slip system from <110>{111} to <110>{100} is raised due to the effect of the vanadium atom dissolving in the Ni_3Al matrix phase.

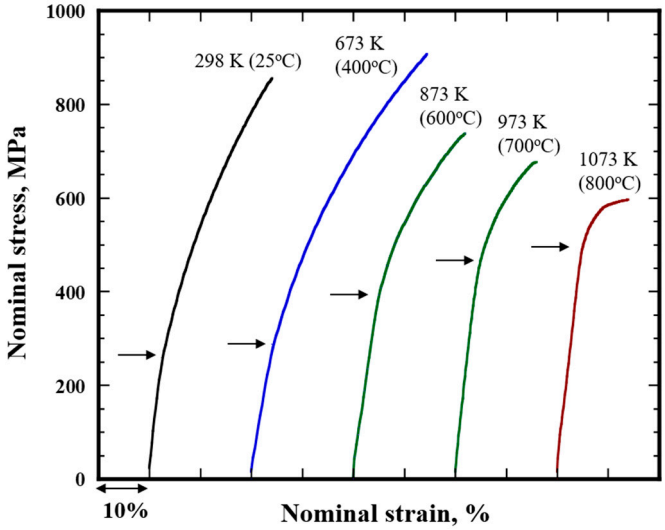


Figure 8. Nominal stress versus nominal strain curves for the Ni_3Al-12V alloy specimens peak-aged at 1123 K for 16 h, measured at temperatures ranging from 298 K to 1073 K.

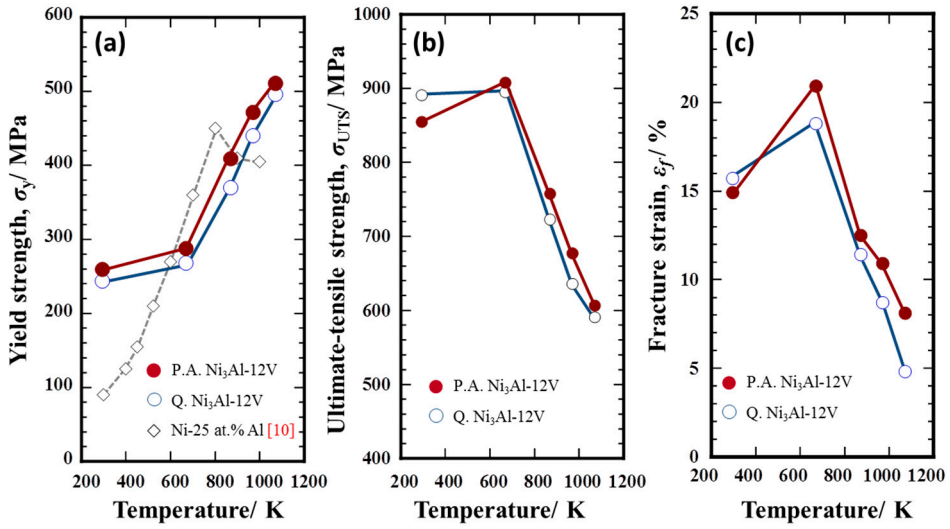


Figure 9. Variations in (**a**) yield strength (0.2% proof stress), (**b**) ultimate tensile strength, and (**c**) fracture strain for the Ni_3Al-12V alloy specimens quenched (Q.) and peak-aged (P.A.) at 1123 K for 16 h as a function of the testing temperature.

The tensile strength and fracture stain for the quenched and peak-aged Ni_3Al-12V alloy specimens were maximum around 673 K, and then decreased monotonically with increasing testing temperature. However, the fracture strain at the highest testing temperature of 1073 K was still above 8% for the peak-aged Ni_3Al-12V alloy specimens, which is a significant improvement compared with the quenched Ni_3Al-12V alloy. Figure 10 shows the FESEM fractographs of the peak-aged Ni_3Al-12V alloy specimen tensile-tested at 298 K and 973 K, together with that of the quenched Ni_3Al-0V tensile-tested at 298 K for comparison. For the former, most areas of the fracture surfaces show a ductile-like dimple pattern (Figure 10a,b). On the other hand, the latter shows a brittle grain boundary facet pattern (Figure 10c), as has been observed in previous studies [2,21,22]. The enhancement in the tensile strength as well as the fracture strain might be attributed to the enhanced grain boundary strength by the V solutes largely dissolving in the Ni_3Al phase via suppressing intergranular fracture. A similar phenomenon has been observed in Ni_3Al alloys containing a large amount of Mn [44,45] and Fe [46], and Ni_3Si containing a large amount of Ti [47]. Moreover, the decrease in both, the tensile strength and fracture strain with increasing testing temperature for the peak-aged Ni_3Al-12V alloy specimen, may be associated with the intrinsic temperature dependence of the Ni_3Al phase matrix, e.g., the transition of the activated slip system [3,43].

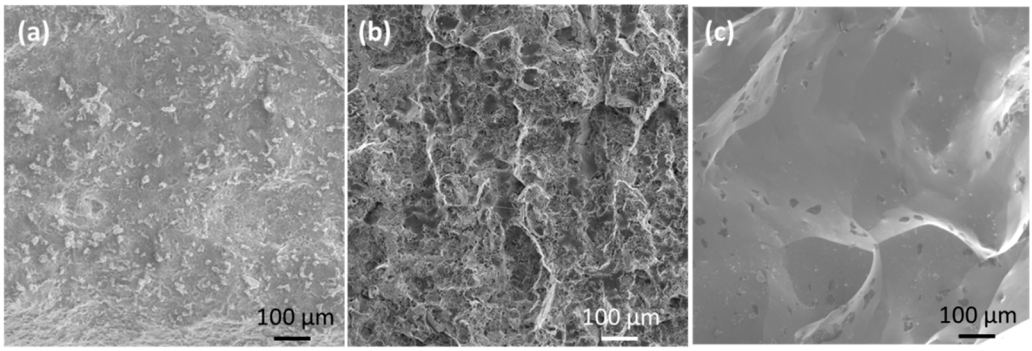


Figure 10. FESEM fractographs for the peak-aged Ni_3Al-12V alloy specimens tensile-tested at (**a**) 298 K and (**b**) 973 K, together with (**c**) that for the Ni_3Al-0V alloy specimens tensile-tested at 298 K.

When comparing the tensile data for the quenched and peak-aged Ni_3Al-12V alloy specimens, the yield strength, ultimate tensile strength, and fracture strain of the aged specimen tended to be superior to those of the quenched specimen, rendering them favorable for application as high-temperature materials. The enhancement in the yield strength and ultimate tensile strength can be explained by age-induced hardening by the $D0_{22}$ Ni_3V precipitates. However, the reason why both the ultimate-tensile strength and fracture strain of the Ni_3Al-12V alloy specimens were improved by aging remains unclear at this stage and is scope for future work.

4. Conclusions

In this study, we investigated the variations in the microstructure and mechanical properties during aging for $L1_2$ Ni_3Al alloy containing a large amount of vanadium (nominal composition of Ni-13 at.% Al-12 at.% V-50 wt. ppm B), which was solution-treated at 1323 K for 48 h in vacuum and then quenched in water. The specimens quenched after solution treatment exhibited a single phase of $L1_2$ Ni_3Al. For the specimens aged at 1123 K after 4 h, a number of fine disk-shaped precipitates were found on {001} planes of the $L1_2$ Ni_3Al matrix. The disk-shaped precipitates were identified as $D0_{22}$ Ni_3V. The size and aspect ratio of the disk-shaped Ni_3V precipitates increased gradually with increasing aging time. The Vickers hardness of the quenched specimen was approximately 280 Hv. During aging at 1073 K to 1173 K, the hardness of the specimens increased and reached a maximum, then decreased. The age-hardening behavior observed for the Ni-13 at.% Al-12 at.% V alloy can be explained in terms of precipitation of the fine disk-shaped Ni_3V phase in the Ni_3Al matrix. The mechanical properties, such as yield strength, ultimate tensile strength, and fracture strain of the

peak-aged Ni-13 at.% Al-12 at.% V alloy specimens at room temperature improved in comparison to the stoichiometric Ni_3Al and quenched Ni-13 at.% Al-12 at.% V alloy. Moreover, the peak-aged alloy showed an anomalous temperature dependency of yield strength up to a maximum testing temperature of 1073 K. These features for the age-hardened Ni-13 at.% Al-12 at.% V alloy are desirable for applications as high-temperature structural materials.

Author Contributions: Conceptualization, S.S.; methodology, S.S. and R.S.; validation, Y.K. and T.T.; formal analysis, R.S.; investigation, R.S.; resources, Y.K.; data curation, S.S. and R.S.; writing—original draft preparation, S.S.; writing—review and editing, T.T.; supervision, T.T.

Funding: This research was funded by the Japan Society for the Promotion of Science (JSPS) as a Grant-in-Aid for Scientific Research (B) (No. 18H01743).

Acknowledgments: The authors thank N. Masahashi of the Institute for Materials Research (IMR) of Tohoku University and A. Iwase of Osaka Prefecture University for constructive discussion and comments. The authors also thank E. Aoyagi, S. Itoh, and I. Nagano of IMR of Tohoku University for their assistance with the experimental work. Technical support provided by the Cooperative Research and Development Center for Advanced Materials (CRDAM) of IMR is also greatly appreciated.

Conflicts of Interest: The authors declare no conflict of interest.

References

1. Noguchi, O.; Oya, Y.; Suzuki, T. The effect of non-stoichiometry on the positive temperature-dependence of strength of Ni_3Al and Ni_3Ga. *Metall. Trans. A* **1981**, *12A*, 1647–1654. [CrossRef]
2. Pope, D.P.; Ezz, S.S. Mechanical properties of Ni_3Al and nickel-base alloys with high volume fraction of γ'. *Int. Metal. Rev.* **1984**, *29*, 136–167.
3. Suzuki, T.; Mishima, Y.; Miura, S. Evaluation of the data for the plastic behavior of $Ni_3(Al,X)$ single-crystals. *Mater. Sci. Eng. A* **1991**, *146*, 245–260. [CrossRef]
4. Webb, G.; Debussac, A.; Antolovich, S.D. An analytical description for the deformation response of Ni_3Al alloys in the anomalous regime. *Metall. Trans. A* **1993**, *24A*, 397–401. [CrossRef]
5. Hirsch, P.B. A new theory of the anomalous yield stress in $L1_2$ alloys. *Philos. Mag. A* **1992**, *65*, 569–612. [CrossRef]
6. Hemker, K.J.; Mills, M.J. Measurements of antiphase boundary and complex stacking-fault energies in binary and B-doped Ni_3Al using TEM. *Philos. Mag. A* **1993**, *68*, 305–324. [CrossRef]
7. Lapin, J. Effect of ageing on the microstructure and mechanical behavior of a directionally solidified Ni_3Al-based alloy. *Intermetallics* **1997**, *5*, 615–624. [CrossRef]
8. Demura, M.; Hirano, T. Stress response by the strain-rate change in a binary stoichiometric Ni_3Al single crystal. *Philos. Mag. Lett.* **1997**, *75*, 143–148. [CrossRef]
9. Demura, M.; Kishida, K.; Suga, Y.; Hirano, T. Room-temperature mechanical properties of cold-rolled thin foils of binary, stoichiometric Ni_3Al. *Metall. Mater. Trans. A* **2002**, *33A*, 2607–2613. [CrossRef]
10. Kruml, T.; Conforto, E.; Lo Piccolo, B.; Caillard, D.; Martin, J.L. From dislocation cores to strength and work-hardening: a study of binary Ni_3Al. *Acta Metall.* **2002**, *50*, 5091–5101. [CrossRef]
11. Wang, G.T.; Ding, H.S.; Chen, R.R.; Guo, J.J.; Fu, H.Z. Effect of current intensity on microstructure of Ni_3Al intermetallics prepared by directional solidification electromagnetic cold crucible technique. *Acta Metall. Sin.* **2017**, *53*, 1461–1468.
12. Nunomura, Y.; Kaneno, Y.; Tsuda, H.; Takasugi, T. Phase relation and microstructure in multi-phase intermetallic alloys based on Ni_3Al-Ni_3Ti-Ni_3V pseudo-ternary alloy system. *Intermetallics* **2004**, *12*, 389–399. [CrossRef]
13. Shibuya, S.; Kaneno, Y.; Yoshida, M.; Takasugi, T. Dual multi-phase intermetallic alloys composed of geometrically close packed Ni_3X (X: Al, Ti and V) type structures-II. Mechanical properties. *Acta Mater.* **2006**, *54*, 861–870. [CrossRef]
14. Kawahara, K.; Kaneno, Y.; Kakitsuji, A.; Takasugi, T. Microstructural factors affecting hardness property of dual two-phase intermetallic alloys based on Ni_3Al-Ni_3V pseudo-binary alloy system. *Intermetallics* **2009**, *17*, 938–944. [CrossRef]
15. Edatsugi, D.; Kaneno, Y.; Semboshi, S.; Takasugi, T. Fine precipitation in channel region of two-phase Ni_3Al and Ni_3V intermetallic alloys containing Mo and W. *Metall. Mater. Trans. A* **2016**, *47A*, 998–1008. [CrossRef]

16. Reed, R.C. *The Superalloys: Fundamentals and Applications*; Cambridge University Press: Cambridge, UK, 2008.
17. Gopinath, K.; Gogia, A.K.; Kamat, S.V.; Balamuralikrishnan, R.; Ramamurty, U. Tensile properties of Ni-based superalloy 720Li: Temperature and strain rate effects. *Metall. Mater. Trans. A* **2008**, *39A*, 2340–2350. [CrossRef]
18. Burns, D.E.; Zhang, Y.; Teutsh, M.; Bade, K.; Aktaa, J.; Hemker, K.J. Development of Ni-based superalloys for microelectromechanical systems. *Scripta Mater.* **2012**, *67*, 459–462. [CrossRef]
19. Smith, T.M.; Bonacuse, P.; Sosa, J.; Kulis, M.; Evans, L. A quantifiable and automated volume fraction characterization technique for secondary and tertiary gamma' precipitates in Ni-based superalloys. *Mater. Charact.* **2018**, *140*, 86–94. [CrossRef]
20. Knowles, A.J.; Reynolds, L.; Vorontsov, V.A.; Dye, D. A nickel based superalloy reinforced by both Ni_3Al and Ni_3V ordered-fcc precipitates. *Scripta Mater.* **2019**, *162*, 472–476. [CrossRef]
21. Aoki, K. Ductilization of $L1_2$ intermetallic compound Ni_3Al by microalloying with boron. *Mater. Trans. JIM* **1990**, *31*, 443–448. [CrossRef]
22. Liu, C.T.; White, C.L.; Horton, J.A. Effect of boron on grain-boundaries in Ni_3Al. *Acta Metall.* **1985**, *33*, 213–229. [CrossRef]
23. Taub, A.I.; Briant, C.L. Composition dependence of ductility in boron-doped, nickel-base $L1_2$ alloys. *Acta Metall.* **1987**, *35*, 1597–1603. [CrossRef]
24. Varin, R.A.; Winnicka, M.B. Plasticity of structural intermetallic compounds. *Mater. Sci. Eng. A* **1991**, *137*, 93–103. [CrossRef]
25. Ochiai, S.; Oya, Y.; Suzuki, T. Alloying behavior of Ni_3Al, Ni_3Ga, Ni_3Si and Ni_3Ge. *Acta Metall.* **1984**, *32*, 289–298. [CrossRef]
26. Mishima, Y.; Ochiai, S.; Suzuki, T. Lattice-parameters of Ni(γ), Ni_3Al(γ') and Ni_3Ga(γ') solid-solutions with additions of transition and B-subgroup elements. *Acta Metall.* **1985**, *33*, 1161–1169. [CrossRef]
27. Mishima, Y.; Ochiai, S.; Hamao, N.; Yodogawa, M.; Suzuki, T. Mechanical-properties of Ni_3Al with ternary addition of transition-metal elements. *Trans. JPN. Inst. Met.* **1986**, *27*, 648–655. [CrossRef]
28. Tain, W.H.; Sano, T.; Nemoto, M. Hardening of ordered γ'-Ni_3(Al,Ti) by precipitation of ordered γ. *Scripta Met.* **1986**, *20*, 933–936.
29. Ma, Y.; Ardell, J.A. Coarsening of γ (Ni–Al solid solution) precipitates in a γ' (Ni_3Al) matrix. *Acta Mater.* **2007**, *55*, 4419–4427. [CrossRef]
30. Arzt, E.; Grahle, P. Dispersion strengthening of disordered and ordered metallic materials: From dislocation mechanisms to new alloys. *Z. Metallkd.* **1996**, *87*, 874–884.
31. Arzt, E.; Behr, R.; Gohring, E.; Grahle, P.; Mason, R.P. Dispersion strengthening of intermetallics. *Mater. Sci. Eng. A* **1997**, *234–236*, 22–29. [CrossRef]
32. Meng, J.; Jia, C.C.; He, Q. Fabrication of oxide-reinforced Ni_3Al composites by mechanical alloying and spark plasma sintering. *Mater. Sci. Eng. A* **2006**, *434*, 246–249. [CrossRef]
33. Kobayashi, S.; Sato, K.; Hayashi, E.; Osaka, T.; Konno, T.J.; Kaneno, Y.; Takasugi, T. Alloying effects on the phase equilibria among Ni(A1), Ni_3Al(L1(2)) and Ni_3V(D0(22)) phases. *Intermetallics* **2012**, *23*, 68–75. [CrossRef]
34. Soffa, W.A.; Laughlin, D.E. High-strength age hardening copper-titanium alloys: redivivus. *Prog. Mater. Sci.* **2004**, *49*, 347–366. [CrossRef]
35. Semboshi, S.; Tsuda, H.; Kanano, Y.; Iwase, A.; Takasugi, T. Thermal conductivity of Ni_3V–Ni_3Al pseudo-binary alloys. *Intermetallics* **2015**, *59*, 1–7. [CrossRef]
36. Ioroi, K.; Kaneno, Y.; Semboshi, S.; Takasugi, T. Effect of transition metal addition on microstructure and hardening behavior of two-phase Ni_3Al-Ni_3V intermetallic alloys. *Materialia*. in press. [CrossRef]
37. Porter, D.A.; Easterling, K.E. *Phase Transformations in Metals and Alloys*, 2nd ed.; CRC Press: Boca Raton, FL, USA, 2004; pp. 110–184.
38. Lumley, R.N.; Polmear, I.J.; Morton, A.J. Interrupted aging and secondary precipitation in aluminium alloys. *Mater. Sci. Technol.* **2003**, *19*, 1483–1490. [CrossRef]
39. Khan, I.N.; Starink, M.J.; Yan, J.L. A model for precipitation kinetics and strengthening in Al-Cu-Mg alloys. *Mater. Sci. Eng. A* **2008**, *472*, 66–74. [CrossRef]
40. Semboshi, S.; Amano, S.; Fu, J.; Iwase, A.; Takasugi, T. Kinetics and equilibrium of age-induced precipitation in Cu−Ti binary alloys. *Metall. Mater. Trans. A* **2017**, *48*, 1501–1511. [CrossRef]

41. Ma, J.; Hornbuckle, B.C.; Karaman, I.; Thompson, G.B.; Luo, Z.P.; Chumlyakov, Y.I. The effect of nanoprecipitates on the superelastic properties of FeNiCoAlTa shape memory alloy single crystals. *Acta Mater.* **1972**, *61*, 3445–3455.
42. Kaneno, Y.; Myoki, T.; Takasugi, T. Tensile properties of $L1_2$ intermetallic foils fabricated by cold rolling. *Int. J. Mater. Res.* **2008**, *99*, 1229–1236. [CrossRef]
43. Suzuki, T.; Mishima, Y.; Miura, S. Plastic Behavior in Ni_3(Al,X) single-crystal-temperature, strain-rate, orientation and composition. *ISIJ Int.* **1989**, *29*, l–23. [CrossRef]
44. Masahashi, N.; Takasugi, T.; Izumi, O. High-temperature strength and ductility of $L1_2$-type Ni_3Al-Ni_3Mn intermetallic compound. *J. Mater. Sci.* **1987**, *22*, 2599–2608. [CrossRef]
45. Masahashi, N.; Takasugi, T.; Izumi, O. High-temperature strength and ductility of recrystallized Ni_3Al-Ni_3Mn alloys. *Metall. Trans. A* **1988**, *19*, 345–352. [CrossRef]
46. Masahashi, N.; Kawazoe, H.; Takasugi, T.; Izumi, O. Phase-relations in the section Ni_3Al-Ni_3Fe of the Al-Fe-Ni system. *Z. Metallkd.* **1987**, *78*, 788–794.
47. Takasugi, T.; Nagashima, M.; Izumi, O. Strengthening and ductilization of Ni_3Si by the addition of Ti elements. *Acta Metall.* **1990**, *38*, 747–755. [CrossRef]



© 2019 by the authors. Licensee MDPI, Basel, Switzerland. This article is an open access article distributed under the terms and conditions of the Creative Commons Attribution (CC BY) license (http://creativecommons.org/licenses/by/4.0/).